Adaptive Admittance Control with Tracking Differentiator for Enhanced Force Tracking in High-Precision Robotic Polishing: Reducing Overshoot and Tracking Errors

Shuoqing Li
School of Automation
Central South University
Changsha, China
234612187@csu.edu.cn

Xinhui Tian
School of Automation
Central South University
Changsha, China
756325698@qq.com

Bin Xie*
School of Automation
Central South University
Changsha, China
xiebin@csu.edu.cn

***Abstract*—Precise force control is essential for contact-intensive tasks such as robotic polishing, as it directly affects surface quality under uncertain environments. Insufficient force reduces material removal efficiency, while excessive force may damage the workpiece or compromise operational safety. To overcome the limitations of conventional admittance control in such scenarios, this paper proposes an improved strategy that introduces a tracking differentiator to smooth step force commands, thereby mitigating overshoot during initial tool–workpiece contact. In addition, an adaptive damping regulation mechanism is designed to enhance steady-state force tracking under environmental disturbances. The stability and convergence of the proposed scheme are rigorously analyzed. The effectiveness of the method is validated in both simulation and physical experiments. In experiments conducted on an FR5 robotic arm, the proposed approach reduces the steady-state tracking error from 1.2 N to 0.2 N and suppresses the initial contact overshoot from 16 N to approximately 12 N. The results demonstrate that the proposed method effectively reduces steady-state error and contact overshoot, providing a reliable solution for high-precision force control in robotic polishing applications.**

***Index Terms*—force track, admittance control, tracking differentiator, adaptive control, robotic polishing.**

I. Introduction

Robotics has evolved from primarily non-contact applications to complex, contact-intensive operations requiring sophisticated interaction control [1]. Robotic polishing, illustrated in Fig. 1, a representative example of these operations, has become an essential component of modern automated production [2].

Effective motion control in interaction tasks relies on comprehensive and precise execution strategies, which in turn require accurate models of both the robot and its environment, along with well-defined parameters. While robot models can typically be established with sufficient precision, accurately modeling the environment remains challenging. Inaccuracies in the environmental model can cause the robot's actual trajectory to deviate from the desired path. In contact tasks involving high-stiffness objects, even small deviations may induce substantial contact forces. As a result, relying solely on position control is often impractical. Therefore, achieving high-quality automated robotic polishing requires precise and smooth contact force control.

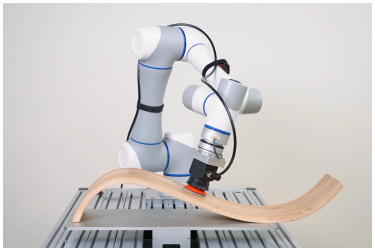

Fig. 1. Robotic polishing applications.

Generally, force control approaches are classified into passive and active methods. Passive force control depends on external devices, while the robot itself usually operates under position control. In contrast, active force control modifies the robot's internal control algorithms, enabling it to directly achieve force servoing.

Impedance control is a typical active force control method, first proposed by Hogan in 1985 [3], that models the robot as a virtual spring–mass–damper system. Admittance control is a position-based approach to implementing impedance control. This method endows the robot with compliance and significantly improves force control during physical interaction [4]. By tuning parameters such as stiffness, inertia, and damping, it enables compliant interaction with the environment and improves force tracking performance during contact-rich tasks.

While impedance control is widely adopted for robotic tasks involving physical interaction with the environment, its force-tracking accuracy is frequently compromised by uncertainties in environmental stiffness and position data [5]. To improve

* Corresponding author.

force tracking performance, various advanced strategies - such as fuzzy control [6], adaptive control [7], and robust control [8] have been integrated into conventional impedance control frameworks. Past research has largely focused on mitigating tracking errors during continuous contact, the initial contact force overshoot often remains a persistent challenge. This overshoot, though transient in nature, can severely compromise system stability and potentially damage either the robot or the workpiece.

This paper aims to enhance force tracking performance in robotic polishing by addressing two key challenges: initial contact overshoot and steady-state tracking errors. The main contributions of this work are as follows:

- A tracking differentiator is employed to smooth the step-like desired force profile during initial contact, effectively suppressing overshoot.
- An adaptive control scheme is proposed to enhance system responsiveness and reduce steady-state tracking errors.

The remainder of this paper is organized as follows. Section II reviews the environmental dynamic model and the baseline admittance control framework. Section III details the design of a tracking differentiator to smooth the step-like desired force input during transient contact. Section IV proposes an adaptive impedance control scheme to compensate for external disturbances, accompanied by detailed stability and convergence analyzes. Section V provides simulation and experimental validation, comparing the force tracking performance of conventional admittance control, adaptive admittance control, and the proposed method. Section VI concludes the paper.

II. System Modeling and Admittance Control Analysis

A. Contact Force Analysis in the Polishing Process

The robot's contact with the workpiece evolves through three sequential states. Initially, in the free state (before t_1), no contact has been made. During the subsequent transition state (t_1 to t_2), contact is initiated, and the force progressively increases from zero. Finally, the interaction reaches the steady state (after t_2), where the contact force stabilizes. The force profile and robot configuration for each state are depicted in Fig. 2 and Fig. 3, respectively.

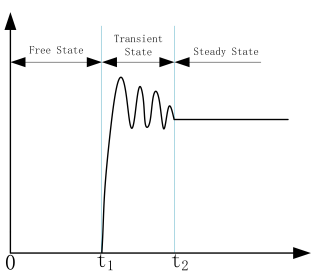

Fig. 2. Contact force profile during the contact process.

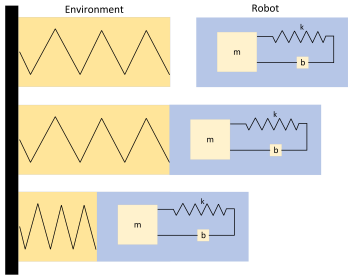

Fig. 3. Three states of Robot–Environment contact.

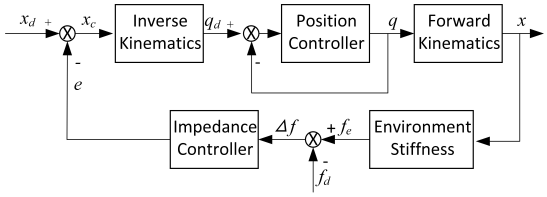

Fig. 4. The scheme of admittance control.

B. Admittance Control Framework

Impedance control can be performed in two main forms: force-based impedance control and position-based impedance control (Admittance Control). Force-based impedance control relies on real-time joint torque feedback, increasing hardware complexity and cost. In contrast, position-based impedance control is generally considered more practical and is widely used in industrial applications.

Fig. 4 illustrates the scheme of admittance control, which employs a dual-loop control architecture. In this structure, the outer loop generates motion position commands designed to achieve the desired admittance characteristics. The inner loop then functions as the robot's position controller, responsible for tracking the commands issued by the outer loop.

For analytical simplicity, the environmental mass M_e and damping B_e are neglected in the dynamic model. The environment is thus modeled as a pure stiffness element:

$$Fe \;=\; K_e\,(X_e - X) \tag{1}$$

Here, K_e denotes the environmental stiffness, X represents the current Cartesian position of the robot, X_e is the environment's equilibrium position, and F_e is the interaction force between the robot and the environment.

This interaction is commonly described by the following second-order differential equation:

$$F_e - F_d = M(\ddot{X}_c - \ddot{X}_d) + B(\dot{X}_c - \dot{X}_d) + K(X_c - X_d) \tag{2}$$

Here, X_d, $\dot{X}_d$, and $\ddot{X}_d$ denote the desired position, velocity, and acceleration, respectively; X_c, $\dot{X}_c$, and $\ddot{X}_c$ represent the position, velocity, and acceleration commands of the robot. M, B, and K are the virtual mass, damping, and stiffness

coefficients, respectively; F_e is the actual contact force, and F_d is the desired contact force.

Let the trajectory correction term be $E(t) = X_c - X_d$, and the controller's transfer function be $K(s) = 1/(Ms^2 + Bs + K)$. Then the actual position command sent to the robot is $X_c = X_d + E = X_d + \Delta F \cdot K(s)$.

C. Performance Analysis of Admittance Control

Conventional admittance control for constant force tracking usually employs fixed parameters for stiffness, mass, and damping. This strategy is inherently limited, as key environmental properties like position and stiffness are difficult to determine accurately in advance. Any mismatch between the preset model and the actual interaction thus degrades force tracking performance, leading to inevitable steady-state errors during the stable contact phase[9, 10].

For ease of analysis, this paper considers single-dimensional force tracking as an example. The force tracking error Δf can be expressed as:

$$\begin{aligned} \Delta f &= f_e - f_d = k_e(x_e - x_c) - f_d \\ &= k_e x_e - k_e(x_d + k(s)\Delta f) - f_d \end{aligned} \tag{3}$$

By substituting $K(s)$ into Equation (3), we obtain:

$$\begin{aligned} &\Delta f(ms^2 + bs + k + k_e) = \\ &(ms^2 + bs + k)[k_e(x_e - x_d) - f_d] \end{aligned} \tag{4}$$

The steady-state error of the system Δf_{ss} is calculated using the Final Value Theorem as follows:

$$\begin{aligned} \Delta f_{ss} &= \lim_{s\to 0} \frac{\left(ms^2 + bs + k\right)\left[k_e\left(x_e - x_d\right) - f_d\right]}{ms^2 + bs + k + ke} \\ &= \frac{k}{k + k_e}[k_e(x_e - x_d) - f_d] \end{aligned} \tag{5}$$

To ensure the steady-state error approaches zero, we must guarantee that:

$$x_d = x_e - \frac{f_d}{k_e} \tag{6}$$

or

$$k = 0 \tag{7}$$

Accurately estimating x_e and k_e is often difficult in practice, making direct compensation based on these parameters impractical. To overcome this, setting $k = 0$ allows for accurate tracking of the desired force:

$$m\ddot{e} + b\dot{e} = \Delta f \tag{8}$$

In robotic control, servo-based motion tracking systems and force sensors are susceptible to transmission delays, control latency, and measurement noise. Furthermore, uncertainties in dynamic model parameters exacerbate force tracking errors. These challenges, largely unaddressed in prior analyses, impede the achievement of high-precision force tracking.

III. Design of Tracking Differentiator

Precise control of contact force necessitates a delicate balance between a rapid response and minimal overshoot. While traditional linear filters can smooth the command signal, they introduce a detrimental trade-off: their inherent phase lag sacrifices system speed and stability for the sake of overshoot suppression.

To resolve this conflict, this work employs a Tracking Differentiator (TD), which functions as a nonlinear trajectory generator rather than a conventional filter.

The TD proactively plans an optimal, smooth transition profile toward the desired force setpoint. Its crucial advantage is achieving this with negligible phase lag, thereby enabling the mitigation of excessive force overshoot during initial contact without compromising the system's rapid transient response [11].

In this paper, the Tracking Differentiator is designed as follows:

$$\begin{cases} f_0 = fhan\left[v_1(k) - f_d(k), v_2(k), r_0, h\right] \\ v_1(k+1) = v_1(k) + hv_2(k) \\ v_2(k+1) = v_2(k) + hf_0 \end{cases} \tag{9}$$

where $f_0 = fhan(x_1, x_2, r_0, h_1)$,

$$\begin{cases} d = r_0 h \\ d_0 = hd \\ y = x_1 + hx_2 \\ a_0 = \sqrt{d^2 + 8r_0|y|} \\ a = \begin{cases} x_2 + \dfrac{a_0 - d}{2}\operatorname{sign}(y), & |y| > d_0, \\ x_2 + \dfrac{y}{h}, & |y| \le d_0 \end{cases} \\ \text{fhan} = -\begin{cases} r\operatorname{sign}(y), & |a| > d_0, \\ r_0\dfrac{a}{d}, & |a| \le d_0 \end{cases} \end{cases} \tag{10}$$

Where f_d is the desired force input, v_1 is the smoothed output, and v_2 is its smoothed derivative. The parameter r_0 governs the transient response speed and is selected based on system performance requirements, while h denotes the control step size. In this simulation, the control step is set to $h = 0.01$, with $f_d = 10N$, and r_0 taking values of 10, 100, and 1000. The corresponding tracking differentiator outputs are shown in Fig. 5.

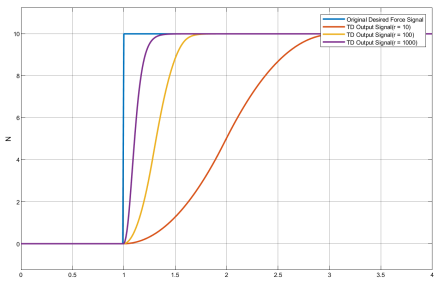

Fig. 5. Simulated response of the tracking differentiator for different values.

IV. Controller Design and Stability Analysis

A. Adaptive Admittance Controller Design

In practical grinding scenarios, the environmental position x_e is often difficult to obtain accurately. Therefore, the concept of an estimated environment is introduced, where the estimated environmental position is defined as the sum of the actual position x_e and a disturbance term δx_e, $\hat{x}_e = x_e + \delta x_e$. Therefore, Equation (8) can be rewritten as:

$$\Delta f = m\ddot{\hat{e}} + b\dot{\hat{e}} = m(\ddot{e} - \delta\ddot{x}_e) + b(\ddot{e} - \delta\dot{x}_e) \tag{11}$$

To compensate for disturbances, an adaptive control algorithm is introduced, which adjusts the damping parameter online based on the historical data of the contact force tracking error. The adaptive admittance control law is expressed as follows:

$$f_e(t) - f_d(t) = m\ddot{\hat{e}}(t) + (b + \Delta b(t))\dot{\hat{e}}(t) \tag{12}$$

where $\Delta b(t)$ represents the adaptive compensation component, which is designed as follows:

$$\begin{cases} \Delta b(t) = \frac{b}{\dot{\hat{e}}(t)}\phi(t) \\ \phi(t) = \phi(t-\lambda) + \sigma\frac{f_d(t-\lambda) - f_e(t-\lambda)}{b} \end{cases} \tag{13}$$

The initial state $\phi(0) = 0$, where λ represents the control period of the system, and σ denotes the update rate. The fundamental concept is to compensate for the tracking error caused by the aforementioned factors within the damping term.

B. Stability and Convergence Analysis

In the previous section, the control law of the adaptive admittance control was provided. In this section, the stability of the system is analyzed and the corresponding constraint conditions are given. Substituting equation (13) into equation (12), we obtain:

$$\begin{aligned} &m\ddot{e}(t) + b\dot{e}(t) + b\Phi(t-\lambda) + \sigma[f_d(t-\lambda) - f_e(t-\lambda)] \\ &- [f_e(t) - f_d(t)] = -m\delta\ddot{x}_e(t) - b\delta\dot{x}_e(t) \end{aligned} \tag{14}$$

According to the environmental stiffness model, substituting equation (1) into equation (14) yields:

$$\begin{aligned} &- m\ddot{f}_e(t) - b\dot{f}_e(t) + bk_e\Phi(t-\lambda) - k_e[f_e(t) - f_d(t)] \\ &+ \sigma k_e[f_d(t-\lambda) - f_e(t-\lambda)] \\ &= -mk_e\delta\ddot{x}_e(t) - bk_e\delta\dot{x}_e(t) \end{aligned} \tag{15}$$

Let:

$$\begin{cases} \widehat{f}_e(t) = k_e\delta\dot{x}_e(t) \\ c(t) = f_d(t) - f_e(t) \\ r(t) = f_d(t) - \hat{f}_e(t) \end{cases} \tag{16}$$

Equation (15) can be rewritten as:

$$\begin{aligned} &m\ddot{c} + b\dot{c} + bk_e\Phi(t-\lambda) + \\ &\sigma k_e c(t-\lambda) + k_e c = m\ddot{r} + b\dot{r} \end{aligned} \tag{17}$$

According to the Laplace transform property:$\mathcal{L}[f(t-\lambda)] = e^{-\lambda s}F(s)$, Applying the Laplace transform to equation (17), we obtain:

$$\frac{c(s)}{r(s)} = \frac{ms^2 + bs}{ms^2 + bs + k_e + \sigma k_e(e^{-(n+1)\lambda s} + \cdots + e^{-\lambda s})} \tag{18}$$

The characteristic equation of the system is:

$$ms^2 + bs + k_e + \sigma k_e(\mathrm{e}^{-(n+1)\lambda s} + \cdots + \mathrm{e}^{-\lambda s}) = 0 \tag{19}$$

Under the assumption that n is a sufficiently large number, it can be expressed as:

$$\sum_{n=1}^{\infty} e^{-\lambda n s} = \frac{e^{-\lambda s}}{1 - e^{-\lambda s}} \tag{20}$$

When the sampling rate λ is sufficient, the delayed term can be approximated as $e^{-\lambda s} \simeq 1 - \lambda s$ by Taylor expansion.Equation (19) can be written as:

$$\lambda m s^3 + \lambda b s^2 + k_e\lambda(1-\sigma)s + \sigma k_e = 0 \tag{21}$$

According to the Routh stability criterion, the constraint conditions for the system stability can be derived as:

$$0 < \sigma < \frac{\lambda b}{m + \lambda b} \tag{22}$$

For a stable system, the steady-state error can be calculated, and the system's steady-state error e_{ss} is given by:

$$\begin{aligned} e_{ss} &= \lim_{t\to\infty} e(t) = \lim_{s\to 0} sE(s) = \lim_{s\to 0} s(c(s) - r(s)) = \\ &\lim_{s\to 0} s\Big[\frac{ms^2 +}{ms^2 + bs + k_e +} \to \\ &\leftarrow \frac{bs}{\sigma k_e(\mathrm{e}^{-(n-1)\lambda s} + \cdots + \mathrm{e}^{-\lambda s})} r(s) - r(s)\Big] \end{aligned} \tag{23}$$

When the system input is a unit step signal, $r(s) = \frac{1}{s}$, we can calculate:

$$e_{ss} = \lim_{s\to 0} s(c(s) - r(s)) = -1 \tag{24}$$

Therefore, we can obtain:

$$\lim_{t\to\infty} c(t) = 0 \tag{25}$$

From equation (25), we observe that as $t \to \infty$, $f_e \to f_d$, indicating that force tracking of the desired force can be achieved.

V. Simulation and Experimental Validation

A. Simulation Validation

To validate the effectiveness of the proposed algorithm, comparative simulations were performed in MATLAB Simulink between admittance control (AC), adaptive admittance control (AAC), and the method proposed in this paper (TD+AAC). The simulations were conducted under three distinct environmental conditions: plane, slope surface and sine surface. To evaluate system performance, experiments were performed under varying environmental conditions. The slope surface and sine surface simulate disturbances resulting from

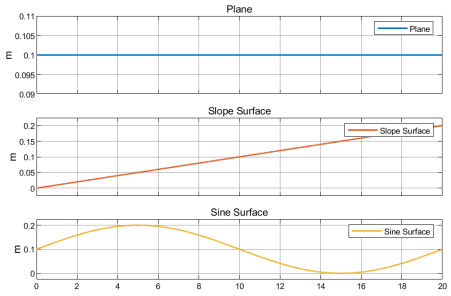

Fig. 6. The environmental positions of the plane, slope surface and sine surface.

environmental position variations, while the introduction of time-varying environmental stiffness accounts for disturbances caused by fluctuations in stiffness.

The workpiece stiffness was set as $k_e = 6000 + 200\sin\left(\frac{\pi t}{4}\right)$ N/m. The admittance controller parameters were set to $m = 1$, $b = 125$, and $k = 0$. The adaptive compensation parameter σ was set to 0.002.The desired contact force was set to 50 N. The environmental position settings for the three experiments are illustrated in Fig. 6.

1) Force Tracking On Plane: When the contact surface is a plane, $\dot{x}_e = 0$ and $\ddot{x}_e = 0$, meaning there is no disturbance in the environmental position. The force tracking results of the three control methods are shown in Fig. 7. Admittance control can achieve effective force tracking on plane, assuming no positional disturbances. However, when adaptive control is integrated, its aggressive response to a step-like desired force signal, aiming for rapid error compensation during initial contact, often induces noticeable overshoot. Introducing a tracking differentiator allows the step-like desired force signal to ramp up smoothly. This approach significantly reduces the initial contact overshoot and also effectively diminishes steady-state tracking error.

2) Force Tracking On Slope Surface: When the contact surface is an inclined plane, $\dot{x}_e \neq 0$ and $\ddot{x}_e = 0$, indicating the presence of environmental position disturbances. The force tracking result is shown in Fig. 8.

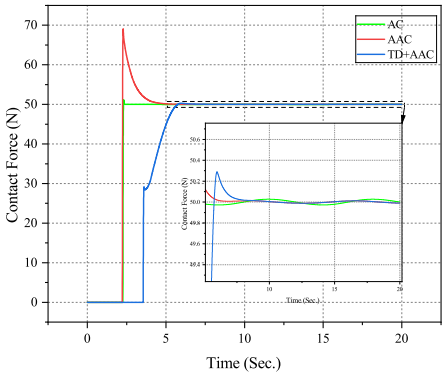

Fig. 7. Result of force tracking on plane.

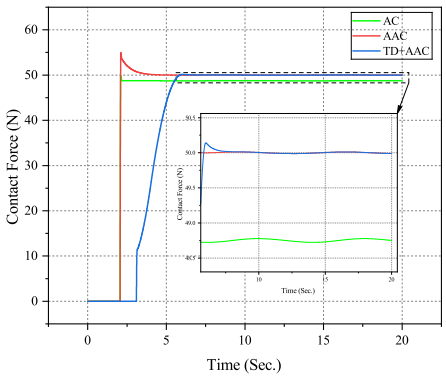

Fig. 8. Result of force tracking on slope surface.

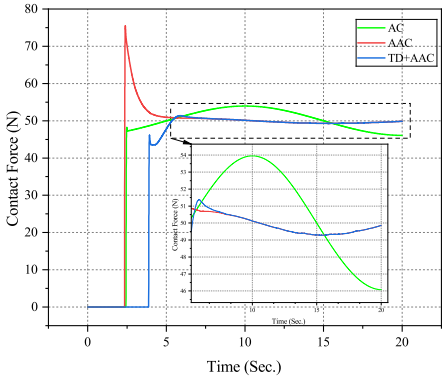

Fig. 9. Result of force tracking on sine surface.

Compared with admittance control, adaptive admittance control effectively reduces the steady-state tracking error but tends to introduce increased overshoot. The method proposed in this paper can effectively reduce the steady-state tracking error while also mitigating the overshoot caused by excessive velocity during the initial contact phase.The steady-state error was reduced from approximately $\pm 1.2\,\mathrm{N}$ to approximately $\pm 0.01\,\mathrm{N}$.

3) Force Tracking On Sine Surface: When the contact surface is a sine surface, $\dot{x}_e \neq 0$ and $\ddot{x}_e \neq 0$, indicating the presence of environmental position disturbances with increased complexity. The force tracking result is shown in Fig. 9. It can be observed that, under significant environmental disturbances, conventional admittance control exhibits large tracking errors. The proposed method can effectively reduce the steady-state tracking error while also limiting the large overshoot caused by disturbance compensation during the initial contact phase. The steady-state error was reduced from approximately $\pm 4\,\mathrm{N}$ to $\pm 0.7\,\mathrm{N}$.

B. Polishing Experiment

The experimental setup consisted of an FR5 robotic manipulator equipped with a six-axis force/torque sensor and a polishing end-effector. After gravity compensation, force tracking experiments were carried out on a steel workpiece. The desired contact force was set to $-10\,\mathrm{N}$.

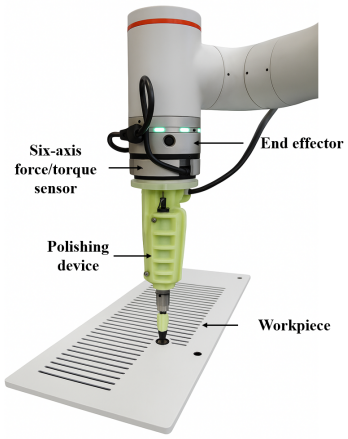

Fig. 10. Polishing experimental apparatus.

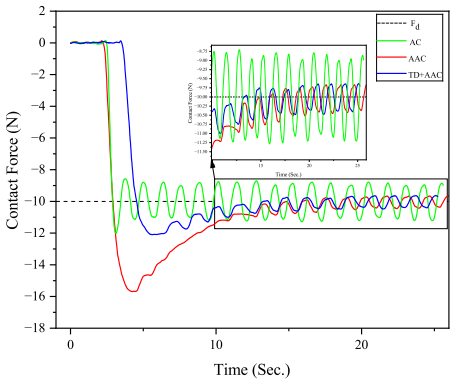

Fig. 11. Result of force tracking on polishing environment.

The admittance controller parameters were configured as $m = 5$ and $b = 50$. The adaptive parameter factor was chosen as $\sigma = 0.002$, and the differential tracker parameter was set to $r_0 = 0.05$. The experimental system is shown in Fig. 10, and the corresponding force tracking results are presented in Fig. 11.

Admittance control exhibits considerable steady-state force tracking errors. By incorporating adaptive admittance control, the steady-state error is significantly reduced from 1.2 N to 0.3 N. However, this improvement is accompanied by an increased force overshoot during the initial contact phase. To address this issue, the proposed method integrates a tracking differentiator into the adaptive admittance control framework, which not only further reduces the steady-state error but also effectively suppresses the initial overshoot from 15.8 N to 12 N thereby demonstrating enhanced force control accuracy and system stability.

VI. Conclusion

Consistent contact force is paramount for high-quality robotic polishing, making accurate force tracking critical. This study proposes an adaptive admittance control to manage uncertainties in polishing environments. Our method dynamically adjusts admittance parameters against tracking errors and employs a tracking differentiator to suppress initial contact overshoot, significantly improving both transient and steady-state performance. Simulations and experiments confirm high-precision force tracking with greatly reduced overshoot during polishing. The framework's robust generalizability suggests its potential for broader contact-intensive tasks requiring precise force control.

References

[1] Xi Zeng, Guangyi Zhu, Zhuohan Gao, Renquan Ji, Juwer Ansari, and Congda Lu. Surface polishing by industrial robots: a review. *The International Journal of Advanced Manufacturing Technology*, 125(9):3981–4012, 2023.

[2] Xiaolong Ke, Yongheng Yu, Kangsen Li, Tianyi Wang, Bo Zhong, Zhenzhong Wang, Lingbao Kong, Jiang Guo, Lei Huang, Mourad Idir, et al. Review on robot-assisted polishing: Status and future trends. *Robotics and Computer-integrated manufacturing*, 80:102482, 2023.

[3] Neville Hogan. Impedance control: An approach to manipulation. In *1984 American control conference*, pages 304–313. IEEE, 1984.

[4] Donghun Lee. Robots in the shipbuilding industry. *Robotics and Computer-Integrated Manufacturing*, 30(5):442–450, 2014.

[5] Inhwan Yoon, Minwoo Na, and Jae-Bok Song. Assembly of low-stiffness parts through admittance control with adaptive stiffness. *Robotics and Computer-Integrated Manufacturing*, 86:102678, 2024.

[6] Qilong Wang, Wei Wang, Lianyu Zheng, and Chao Yun. Force control-based vibration suppression in robotic grinding of large thin-wall shells. *Robotics and Computer-Integrated Manufacturing*, 67:102031, 2021.

[7] Yuzhu Sun, Mien Van, Stephen McIlvanna, Nhat Nguyen Minh, Seán McLoone, and Dariusz Ceglarek. Adaptive admittance control for safety-critical physical human robot collaboration. *IFAC-PapersOnLine*, 56(2):1313–1318, 2023.

[8] Seung Jae Lee, Seung Hyun Kim, and Hyoun Jin Kim. Robust translational force control of multi-rotor uav for precise acceleration tracking. *IEEE Transactions on Automation Science and Engineering*, 17(2):562–573, 2019.

[9] Raouf Fareh, Sofiane Khadraoui, Mahmoud Y Abdallah, Mohammed Baziyad, and Maamar Bettayeb. Active disturbance rejection control for robotic systems: A review. *Mechatronics*, 80:102671, 2021.

[10] Hongli Cao, Xiaoan Chen, Ye He, and Xue Zhao. Dynamic adaptive hybrid impedance control for dynamic contact force tracking in uncertain environments. *Ieee Access*, 7:83162–83174, 2019.

[11] Gabriel Aguirre-Ollinger and Haoyong Yu. Lower-limb exoskeleton with variable-structure series elastic actuators: Phase-synchronized force control for gait asymmetry correction. *IEEE Transactions on Robotics*, 37(3):763–779, 2020.